Differential Helix Stabilities and Sites Pre-organized for Tertiary Interactions Revealed by Monitoring Local Nucleotide Flexibility in the bI5 Group I Intron RNA†

Stacy I. Chamberlin‡ and Kevin M. Weeks*

Department of Chemistry, University of North Carolina, Chapel Hill, North Carolina 27599-3290

Received September 8, 2002; Revised Manuscript Received November 11, 2002

ABSTRACT: The local environment at adenosine residues in the bI5 group I intron RNA was monitored as a function of Mg^{2+} using both the traditional method of dimethyl sulfate (DMS) N1 methylation and a new approach, selective acylation of 2′-amine substituted nucleotides. These probes yield complementary structural information because N1 methylation reports accessibility at the base pairing face, whereas 2′-amine acylation scores overall residue flexibility. 2′-Amine acylation robustly detects RNA secondary structure and is sensitive to higher order interactions not monitored by DMS. Disruption of RNA structure due to the 2′-amine substitution is rare and can be compensated by stabilizing folding conditions. Peripheral helices that do not interact with other parts of the RNA are more stable than both base paired helices and tertiary interactions in the conserved catalytic core. The equilibrium state of the bI5 intron RNA, prior to assembly with its protein cofactor, thus features a relatively loosely packed core anchored by more stable external stem−loop structures. Adenosine residues in J4/5 and P9.0 form structures in which the nucleotide is constrained but the N1 position is accessible, consistent with pre-organization to form long-range interactions with the 5′ and 3′ splice sites.

Large scale and facile detection of the local environment at individual nucleotides in RNA is invaluable for guiding structure prediction and for understanding RNA folding reactions. One good starting point for a global analysis of local nucleotide environments in RNA are adenosine residues, which are over represented among both important local and tertiary motifs. Adenosine nucleotides form A·A, A·C, and A·G noncanonical base pairs (*1*−*3*), A-platforms (*4*), and long-range interactions, often via the minor groove (*5*, *6*).

A traditional approach for monitoring RNA structure is base alkylation by the electrophilic reagent dimethyl sulfate (DMS) (*7*). DMS methylates the N1 of adenosine, N3 of cytosine, and N7 of guanosine (illustrated for N1 of adenosine in Figure 1B) and is commonly used to monitor the base pairing interactions that define RNA secondary structure (*8*). DMS is relatively insensitive to noncanonical and higher order contacts, because many of these interactions do not involve the N1, N3, or N7 position of A, C, or G, respectively.

Alternatively, acylation of 2′-amine substituted RNA is a robust approach for monitoring local nucleotide flexibility and folding transitions in RNA (*9*, *10*). 2′-Amine acylation is broadly sensitive to local nucleotide flexibility such that residues constrained by structural contacts are unreactive even if the 2′-ribose position is solvent accessible (Scheme 1, Figure 1A). For example, residues constrained by either base pairing or higher order tertiary contacts are detected in $tRNA^{Asp}$ as reduced 2′-amine reactivities (*9*).

The mechanism by which N1 methylation is sensitive to base pair formation at adenosine residues can be understood in a straightforward way. In a canonical base pair, the N1 of adenosine is directly involved in forming an interbase hydrogen bond and is inaccessible (Figure 1C). A more complex mechanism is required to explain the physical basis by which 2′-amine substitutions become unreactive when a nucleotide is constrained by base pairing, since the 2′-ribose position is accessible to solvent in helical RNA. We proposed (*9*) and model studies support (*11*) a mechanism in which the nucleophilicity of the 2′-amine is enhanced by interacting with the adjacent RNA phosphodiester group (Scheme 1). 2′-Amine acylation reports local flexibility because flexible nucleotides can more readily achieve the local conformation required for intramolecular catalysis by the 3′-phosphodiester.

In this work, we explore 2′-amine acylation as a tool for monitoring RNA structure by comparing this chemistry to the traditional RNA structure probe, DMS, using the yeast mitochondrial bI5 group I intron RNA. The catalytic core of the bI5 group I intron folds into a well-defined structure formed by two roughly coaxially stacked domains comprised of helices P5−P4−P6 and P7−P3−P8 (*12*−*14*) (see Figures 4 and 5). These core helices form a catalytic cleft that binds a third helical structure (P1−P2) that includes the 5′ splice site. An exogenous guanosine nucleophile, that initiates the splicing reaction, binds in P7. Like other large RNAs, the bI5 group I intron is replete with adenosine rich motifs, such as adenosine platforms, a GAAA tetraloop, sheared A·A base pairs, and A-minor interactions.

* Corresponding author, email: weeks@unc.edu.

† Supported by grants from the NIH (GM56222) and NSF (MCB9984289) and by a Research Innovation Award (Research Corp.) to K.M.W.

‡ Current Address: Department of Biochemistry, Duke University Medical Center, Durham, NC 27710.

10.1021/bi026817h CCC: $25.00
Published on Web 01/08/2003

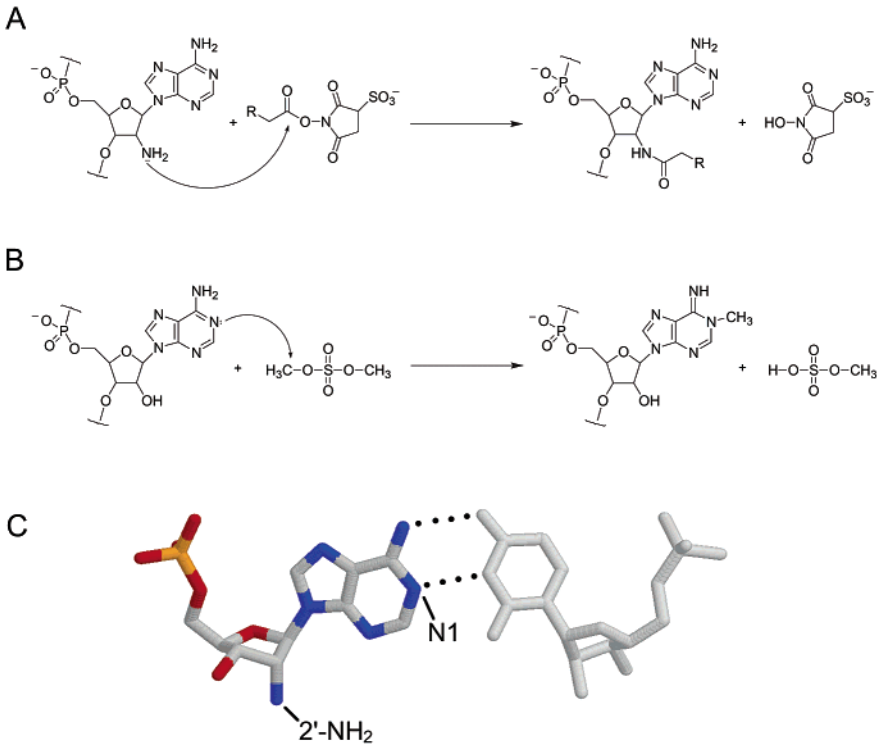

FIGURE 1: 2′-Amine acylation and N1 base methylation as probes of local RNA structure at adenosine residues. (A) Selective acylation of a 2′-amine with a succinimidyl ester to yield the 2′-amido product. (B) Reaction at the N1 position of adenosine by DMS. After forming an initial N^+-CH_3 lesion, the methylated base resolves to the tautomer shown (*19*). (C) Structure of an A·U base pair and the sites involved in 2′-amine acylation and N1 methylation chemistries.

Scheme 1

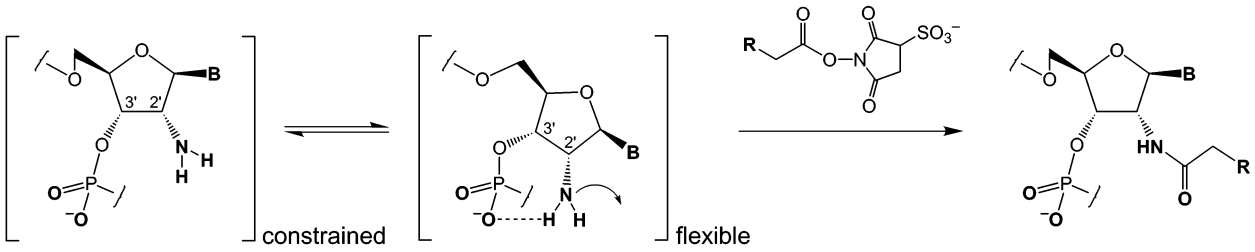

These studies emphasize that 2′-amine acylation is a robust probe of RNA structure and monitors many interactions refractory to detection by DMS methylation. Second, our results support a model for the bI5 intron-derived RNA in which external helices with phylogenetically variable sequences are more stable than structures containing conserved motifs that form the closely packed catalytic core. Finally, structures in J4/5 and P9.0 are locally constrained and potentially preorganized to form long-range tertiary interactions with the 5′ and 3′ splice sites.

EXPERIMENTAL SECTION

bI5 RNA Synthesis. bI5 transcripts were synthesized enzymatically using T7 RNA polymerase and a plasmid template (pbI5−5R) (*14*) linearized with *Xba I*. The RNA spanned the complete intron shown in Figure 4 and included 5′ and 3′ exons of 35 and 55 nts. Transcription reactions (500 μL, 37 °C, 4 h) for 2′-amine substituted RNAs contained 40 mM Tris (pH 8.0), 15 mM $MgCl_2$, 10 mM dithiothreitol (DTT), 2 mM spermidine, 0.01% Triton X-100, 4% poly(ethylene glycol) 8000, 25 μg of linearized plasmid, 0.1 mg/mL T7 RNA polymerase, 2 mM CTP, GTP, and UTP, 0.8 mM ATP, and 1.2 mM 2′-amino-2′-deoxy ATP and yield transcripts substituted with 2′-amino nucleotides at the 2% level (*9*). DMS modification experiments employed all ribose (2′-OH) RNAs; transcription reactions (500 μL; 37 °C, 4 h) contained 80 mM Hepes (pH 7.6), 10 mM $MgCl_2$, 40 mM DTT, 2.5 mM each nucleotide triphosphate, and the same concentrations of Triton, spermidine, plasmid, and polymerase as above. RNAs were purified by denaturing electrophoresis (90 mM Tris-borate, 2 mM EDTA, 7 M urea, 4% 29:1 acrylamide/bisacrylamide); excised from the gel; recovered by elution overnight into 500 mM potassium acetate (pH 6.0); precipitated with ethanol; resuspended in TE (10 mM Tris, pH 7.5, 1 mM EDTA); and stored at −20 °C.

RNA Modified Under Denaturing Conditions. RNA (1 pmol, 1 μL) in 100 mM Hepes (pH 7.6), 1 mM EDTA and 50% (v/v) formamide was heated to 95 °C for 1 min, treated with 1 μL of sulfosuccinimidyl-6-(biotinamido)hexanoate (Pierce, 500 mM in DMSO, 10 μL total reaction volume) or DMS (1:50 in EtOH), and incubated at 50 °C for 5 min. Control reactions contained 1 μL of DMSO or EtOH lacking reagent. Reactions were quenched by addition of 90 μL of

Table 1: bI5 RNA Structure as a Function of Folding Conditions

condition	symbol	state
50% formamide, 1 mM EDTA	D	denatured
0 mM $MgCl_2$ [a]	0	expanded (*16*), with partial base pairing
7 mM $MgCl_2$ [a]	7	collapsed (*16*), with stable base pairing
40 mM $MgCl_2$ [a]	40	Fully folded catalytic core, but 5′-domain not stably associated with core (*15*)

[a] Complete solution conditions (35 °C) included 100 mM Hepes, pH 7.6, and 50 mM KCl.

a 55 mM DTT, 220 mM NaCl and 220 μg/mL glycogen solution followed by precipitation with ethanol and storage in 7 μL of TE at −20 °C.

RNA Modification as a Function of [$MgCl_2$]. RNA (1 pmol, 1 μL) was denatured by heating at 90 °C for 3 min in TE, placed on ice for 5 min, and refolded by incubation (35 °C, 10 min) in 100 mM Hepes (pH 7.6), 50 mM KCl and 0, 7, or 40 mM $MgCl_2$. Chemical modification (35 °C, 5 min) and control reactions were initiated, quenched, and processed as outlined above.

Primer Extension. Reverse transcriptase mediated primer extension reactions were identical to those described previously (*9*). Oligonucleotide primers were complimentary to positions 130−150, 213−232, 279−304, or the 3′ end of the RNA. Reactions were resolved on denaturing gels (8% polyacrylamide, 0.75 mm × 28.5 cm × 38.5 cm, 70 W) electrophoresed for 2 or 3.5 h to resolve cDNA products approximately 2−75 and 75−150 nucleotides longer than the primer, respectively. Band intensities were visualized and quantified using a Phosphorimager (Molecular Dynamics). Sample loading was normalized to an internal background band corresponding to an unmodified position in the sequence. Variations in band intensities, due to background modification, degradation, and less than perfect sample loading, were taken into account when interpreting data. All data interpretations represent a consensus protection pattern from three or more independent experiments and, for some residues, resolution by multiple primers.

RESULTS

Strategy. The structure of the bI5 RNA can be manipulated into distinct folded states by varying magnesium ion concentrations in vitro (summarized in Table 1) (*15*, *16*). In the absence of Mg^{2+}, the bI5 RNA is in a conformationally expanded state (*16*) and, as will be shown in this work, is characterized by incomplete base pair formation. At 7 mM Mg^{2+}, the bI5 catalytic core is predominately in an on-pathway, but non-native, collapsed state and has a stable secondary structure (*15*−*17*). This collapsed state has a Stokes radius only 10% larger than the native state, but does not fold to form a solvent inaccessible catalytic core (*16*). Native folding of the catalytic core requires high magnesium ion concentrations (40 mM Mg^{2+}). The 5′ splice site domain (P1−P2−P2a) does not stably associate with the catalytic core at 40 mM Mg^{2+}, or under any conditions employed in this work. Stable association of the 5′ splice site with the catalytic core requires binding by the protein cofactor, CBP2 (*15*, *18*).

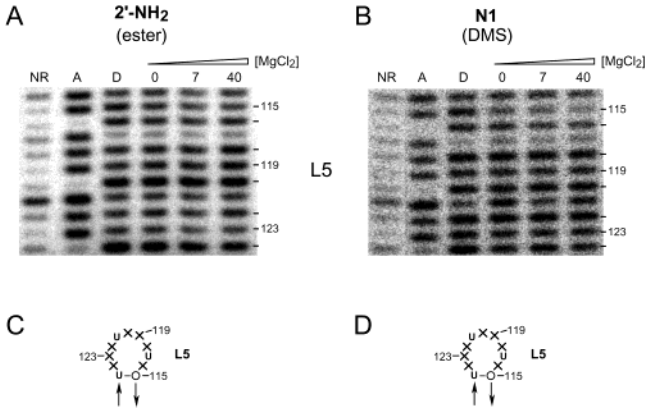

FIGURE 2: 2′-Amine acylation and N1 methylation chemistries are intrinsically insensitive to Mg^{2+}. Representative data for the flexible L5 loop region are shown for (A) acylation of 2′-amine substituted and (B) methylation of all-ribose bI5 RNA. Reactivities for RNAs modified at 0, 7, and 40 mM $MgCl_2$ are similar to those for denatured RNAs (lane D). 2′-Amido and N1-methyl adenosine modifications were detected by primer extension and are offset by one position relative to the dideoxy adenosine sequencing lane (lane A). All adenosine positions are indicated with tic marks at right. Reactions in the absence of succinimidyl ester or DMS (NR lanes) control for RNA degradation and sequence specific stops to primer extension. Changes in relative reactivity are summarized on the local secondary structure for (C) 2′-amine acylation and (D) N1 methylation. × and ○ indicate no change in reactivity or modest protection at 0 mM Mg^{2+}, as compared with reactivity under denaturing conditions, respectively. Arrows indicate 5′ to 3′ direction of the sequence.

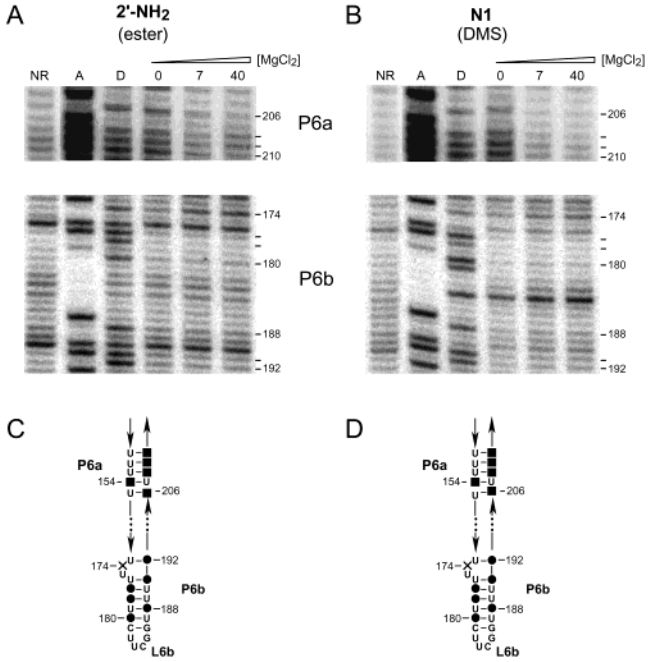

FIGURE 3: Canonical base pairs yield similar 2′-amine acylation (A) and N1 methylation (B) protection patterns. Reactions were performed at 0, 7, and 40 mM $MgCl_2$. D indicates denaturing conditions; A is a dideoxy sequencing ladder; and NR indicates control reactions omitting reagent. Folding transitions are summarized on the local secondary structure for 2′-amine acylation (C) and N1 methylation (D). Filled circles and squares indicate strong protection at 0 and 7 mM $MgCl_2$, respectively.

We compared the extent of local structure under each of these distinct folded states (0, 7, 40 mM Mg^{2+}; Table 1) with control reactions in which the RNA was completely denatured (50% formamide). The local environment at each

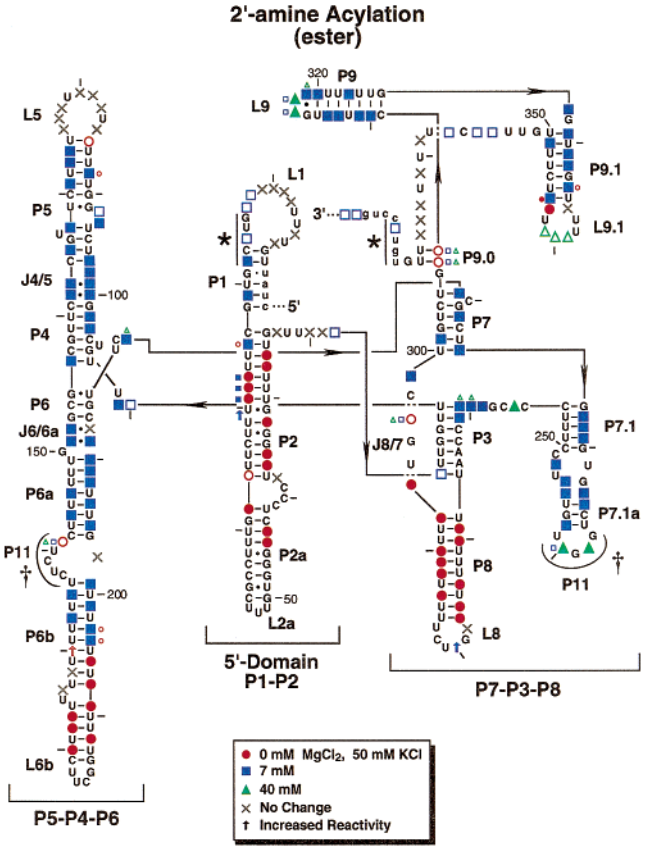

FIGURE 4: bI5 RNA folding transitions monitored by acylation of 2′-amine substituted nucleotides. Adenosine residues are represented by symbols indicating the solution condition at which the nucleotide is protected from acylation (see box). Solid and open symbols indicate strong and moderate-to-weak protection, respectively. Large symbols refer to the predominant folding transition at positions where multiple or broad transitions are detected. Adenosine residues reactive under all conditions are shown by an ×; arrows indicate an increase in reactivity. Protection patterns are reported as a consensus from at least three independent experiments; a few residues yielding inconsistent data are represented by A. The P10 and P11 helices are indicated with an asterisk and dagger, respectively.

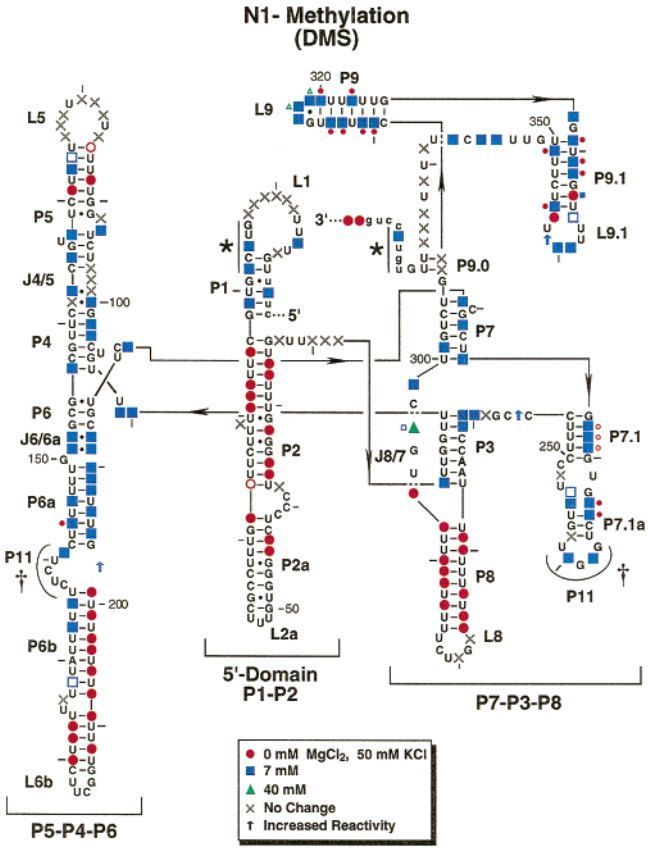

FIGURE 5: bI5 RNA folding transitions monitored by N1 base methylation using DMS. For symbols and methods see legend to Figure 4.

adenosine residue was probed by 2′-amine acylation and DMS methylation, which are sensitive to local nucleotide flexibility (*9*, *11*) and the solvent accessibility of the N1 position (*8*, *19*), respectively. 2′-Amine acylation experiments (Figure 1A) employed transcripts sparsely substituted with 2′-amino adenosine. DMS methylation (Figure 1B) was performed with all-ribose RNAs. Modified adenosine positions (2′-amido or N1-methyl) were detected as stops to primer extension by reverse transcriptase.

2′-Amine Acylation and N1 Methylation are Chemically Insensitive to [Mg^{2+}]. Adenosine residues in the peripheral L5 loop are not involved in interactions with each other or with other regions of the RNA (*12*, *14*, *15*). All 2′-amine and N1 adenosine positions in L5 are reactive under denaturing conditions and also in the presence of increasing Mg^{2+} concentrations (compare D, 0, 7, and 40 lanes in Figure 2A,B, respectively; reactive positions are indicated with an × in Figure 2C,D). Thus, both chemistries are insensitive to Mg^{2+} concentration and observed protection from 2′-amine or N1 modification can be attributed to the local structural environment or to occlusion of the reagents due to RNA folding.

2′-Amine Acylation and N1 Methylation Report the Same Differential Stabilities in Simple Helices. The P6a−P6b region of the bI5 RNA forms a long A−U rich set of helices. Under denaturing (D) conditions, we observe roughly uniform reactivity at all positions (compare D and NR, no reaction, lanes in Figure 3A,B). Two distinct, ion-induced folding transitions are identifiable for base paired regions using either chemistry. Base paired residues in P6b, adjacent to the stable UUCG tetraloop, are unreactive at 50 mM KCl (compare D and 0 lanes in Figure 3A,B; summarized as filled circles in Figure 3C,D). In contrast, base paired residues in P6a remain reactive in the absence of Mg^{2+} (at 50 mM KCl) but are protected at 7 mM Mg^{2+} (compare 0 and 7 lanes in Figure 3A,B; summarized as filled squares in Figure 3C,D). Both chemistries score the unpaired, bulged A at position 174 as reactive under all conditions. Thus, both 2′-amine acylation and DMS methylation reliably detect canonical base pairing. Moreover, individual helices in the bI5 RNA clearly exhibit non-uniform stabilities (circles and squares in Figure 3C,D).

bI5 RNA Folding Transitions Detected by 2′-Amine Acylation and N1 Methylation. Relative reactivities for 2′-amine acylation and DMS methylation could be assessed for almost all adenosine residues in the bI5 RNA under denaturing conditions and in the presence of 0, 7, or 40 mM $MgCl_2$. Consensus reactivity patterns for 2′-amine acylation and N1 methylation are summarized in Figures 4 and 5, respectively.

Inspection of Figures 4 and 5 emphasizes that 2′-amine acylation and N1 methylation detect identical folding transitions for most adenosine residues in the bI5 RNA. In the

Table 2: Structural Interpretations of 2′-Amine Acylation and N1 Methylation at Adenosine Residues

protection from			
2′-amine acylation	DMS methylation	class	interpretation
−	−	1	No interactions. Base is accessible and residue is flexible.
+	+	2	A- Interaction with N1 face of base. Residue constrained. B- Nucleotide inaccessible in folded state.
+	−	3	Nucleotide is conformationally restrained via interactions not involving N1.
−	+	4	A- 2′-amine substitution disrupts local secondary structure. B- Base pairing face inaccessible, nucleotide is flexible.

presence of monovalent ion (50 mM KCl) peripheral structures including P6b, P8, and P2−P2a are protected from both 2′-amine and N1 modification (Figures 4 and 5, red circles).

Essentially all adenosine residues that form conserved elements in the catalytic core require 7 mM Mg^{2+} to form stable base pairs or other local interactions (blue squares in Figures 4 and 5). Only a few positions require high Mg^{2+} concentrations (40 mM) to become protected from modification by either chemistry (green triangles in Figures 4 and 5). These results are consistent with prior work using both 1-cyclohexyl-N^1-(2-*N*-methylmorpholino)ethyl carbodiimide-*p*-toluene sulfonate (CMCT) (*20*) and DMS (*15*) base modification showing that protection patterns are largely unchanged at Mg^{2+} concentrations greater than 5 mM.

Finally, a significant subset of residues are incrementally protected with increasing Mg^{2+} concentration, indicating multiple or broad folding transitions (indicated by small symbols in Figures 4 and 5). The most striking example involves residues within the L9 tetraloop in which A318 and A319 are partially protected from both 2′-amine acylation and N1 methylation at 7 mM Mg^{2+} and then become further protected at 40 mM Mg^{2+}. The L9 tetraloop makes an important long-range tertiary interaction with the P5 helix (*16*, *21*, *22*) and the observed multiple transitions suggest this interaction is incrementally stabilized over a broad range of Mg^{2+} concentrations.

Differences between 2′-Amine Acylation and N1-Methylation Occur in Regions Important for Higher Order Folding. Given that 2′-amine acylation is sensitive to local nucleotide flexibility and DMS reactivity is related more simply to base accessibility, differences in observed protection patterns are expected (summarized in Table 2). Strikingly, most differences between these two structure-sensitive chemistries occur at residues previously implicated in forming higher order interactions. Many of these regions contain important adenosine-rich motifs that are responsible for stabilizing the folded RNA (*12*, *22*) or are important for positioning docking the 5′ and 3′ splice sites (*15*, *23*, *24*). These differences are discussed by RNA region below.

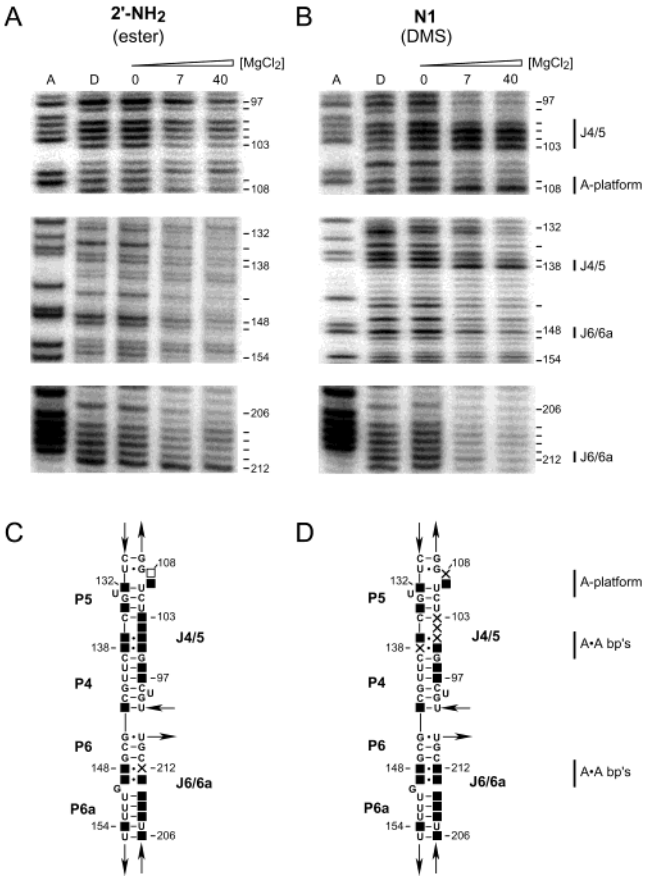

FIGURE 6: Folding of the P5−P4−P6 region in the bI5 intron. Reactions were performed at 0, 7, and 40 mM $MgCl_2$ for 2′-amine acylation (A) and N1 methylation (B). Regions of special interest are identified at the right in B. D indicates denaturing conditions and A is a dideoxy sequencing ladder. Summary of folding transitions detected by 2′-amine acylation (C) and N1 methylation (D). Symbols are identical to those used in Figures 4 and 5 and represent a consensus from multiple data sets.

A·A Pairs in the P5−P4−P6 Domain. The J4/5 region in the P5−P4−P6 domain forms two sheared A·A base pairs (Figure 7A; A101·A137 and A100·A138) capped by a stacked adenosine. This motif is conserved in the same domain of the *Tetrahymena* ribozyme, where the structure has been solved at high resolution (*22*). In the bI5 RNA, all adenosine residues in J4/5 are strongly protected from 2′-amine acylation at 7 mM Mg^{2+} (Figure 6A,C). Uniform protection is consistent with each A forming a stable, well stacked, although non-canonical, base pair (Figure 7A).

N1 methylation yields a different overall pattern of modification in J4/5. Residues 100 and 137, whose base pairing faces stack on each other (Figure 7A), are protected from N1 methylation in the presence of Mg^{2+} (Figure 6B, compare D and 0 lanes with 7 and 40 lanes). The observed parallel protection from 2′-amine acylation and N1 methylation at A100 and A137 represents class 2 (Table 2).

In contrast, the N1 positions of A101 and 138 are exposed in a wide minor groove (Figure 7A) and are accessible to DMS under all conditions tested (Figure 6B,D). These DMS accessible residues interact with the conserved G−U base pair at the 5′ splice site and function to position the splice site helix in the catalytic cleft (*12*, *25*). The lack of DMS protection at A101 and A138 is consistent with the absence of P1 docking in the bI5 intron (*15*). 2′-Amine acylation and

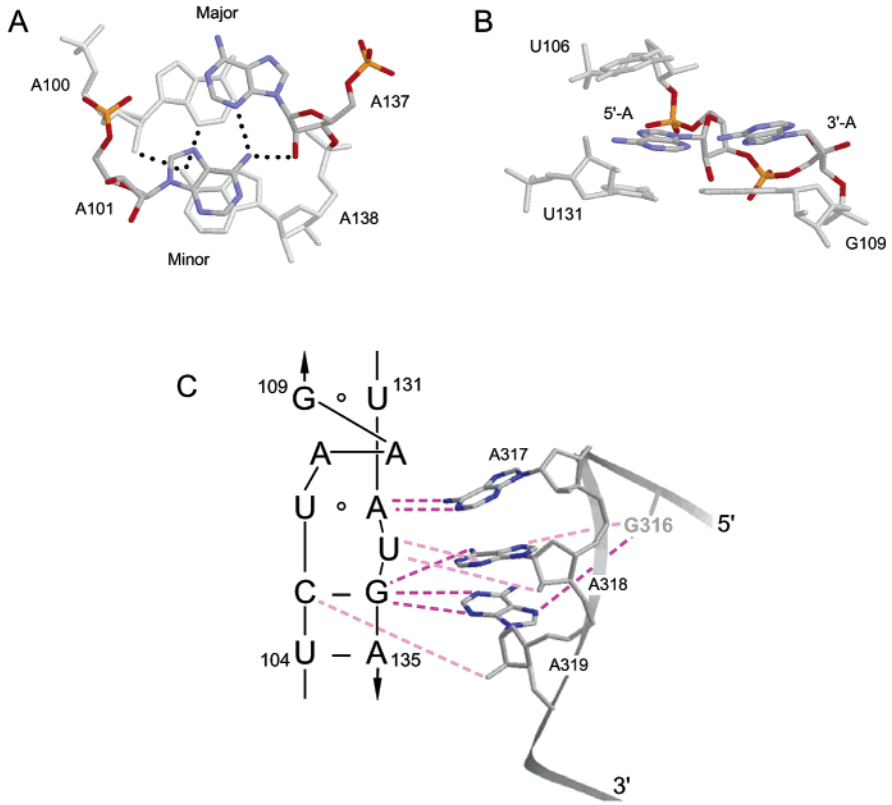

FIGURE 7: Structures of non-canonical interactions in J4/5, P5, and L9. Structures are adapted from homologous regions in the *Tetrahymena* intron (*4*), and are numbered according to the bI5 RNA convention. (A) Sheared A·A base pairs in J4/5. (B) The adenosine platform in P5. (C) Docking of the L9 tetraloop with the receptor in P5. Hydrogen bonding (dashed lines) involving the bases only or mediated by a 2′-OH partner is shown in dark and light magenta, respectively.

N1 methylation recapitulate exactly the structures at A101 and A138, as extrapolated from the *Tetrahymena* domain structure. These residues in J4/5 represent a class 3 protection pattern (Table 2) and may be pre-organized for subsequent interaction with the 5′ splice site.

A second set of A·A mismatches lies in J6/6a in the P5−P4−P6 domain. J6/6a in the *Tetrahymena* intron adopts a helical conformation with a wide minor groove that interacts with P3 in the P7−P3−P8 domain (*13*). A148 and A149 are conserved among group I introns (*12*) and are protected from hydroxyl radical cleavage under conditions in which the bI5 catalytic core is stably folded (*15*, *16*). All adenosine N1 positions are protected from DMS methylation at 7 mM Mg^{2+} (Figure 6). Three of the four adenosine residues within this sequence are protected from 2′-amine acylation at 7 mM Mg^{2+} (Figure 6A,C); lack of consistent protection at A212 may reflect destabilization of the A212·A148 pair or disruption of an interaction with P3 by the 2′-amino adenosine (class 4B, Table 2).

Adenosine Platform and L9-P5 Motifs. The bI5 RNA contains a copy of the common GAAA tetraloop−receptor interaction (*21*, *22*) in a position conserved among a subset of group I introns (*12*, *21*). Two distinct interactions in this motif are instructive for analysis by 2′-amine acylation and DMS methylation.

In the first feature, P5 contains an example of an A-platform (Figure 7B) in which consecutive A residues form a planar pseudo-base pair, stabilized predominantly by base stacking interactions (*4*). The 5′-A (A107) stacks with bases on both sides (Figure 7B) and the 3′-A (A108) stacks primarily with the 3′-guanosine residue. 2′-Amine acylation correctly reports these differential stabilizing interactions as greater protection of the 5′ as compared with the 3′-A (Figure 6A,C), even though the 2′-ribose position is accessible at both residues (Figure 7B).

The second component of this motif involves a series of interactions between stacked adenosine bases from the tetraloop in L9 and the widened minor groove in P5 (Figure 7C). A319 and A318 participate in type I and type II A-minor motifs (*5*, *6*), respectively. As judged by both 2′-amine acylation and N1 methylation, docking of the L9 tetraloop with P5 proceeds in stages (Figure 8, squares and triangles in C and D). Both A318 and 319 are partially protected from 2′-amine acylation and N1 methylation at 7 mM Mg^{2+} and show additional protection at 40 mM. Based on the high-resolution structure of an identical sequence in the *Tetrahymena* ribozyme, A318 and A319 are buried within tightly packed environments (Figure 7C) and form long-range interactions involving their 2′-hydroxyl groups. Close agreement between transitions detected by the two chemistries emphasizes that the 2′-amine substitution does not significantly perturb these interactions. The only position in the tetraloop−receptor interaction that shows possible interference by the 2′-amine group is A317, where strong protection from 2′-amine acylation is shifted to higher (40 mM) Mg^{2+} concentration (Figure 8). Even though the 2′-ribose position is solvent accessible (Figure 7C), A317 appears to be a case in which the 2′-amine substitution may be incompatible with the local RNA structure (class 4, Table 2).

Pre-organization of the 3′ Splice Site. Adenosine residues in the P9.0 helix base pair with the 3′ end of the RNA and position the 3′ splice site within the active site cleft for the

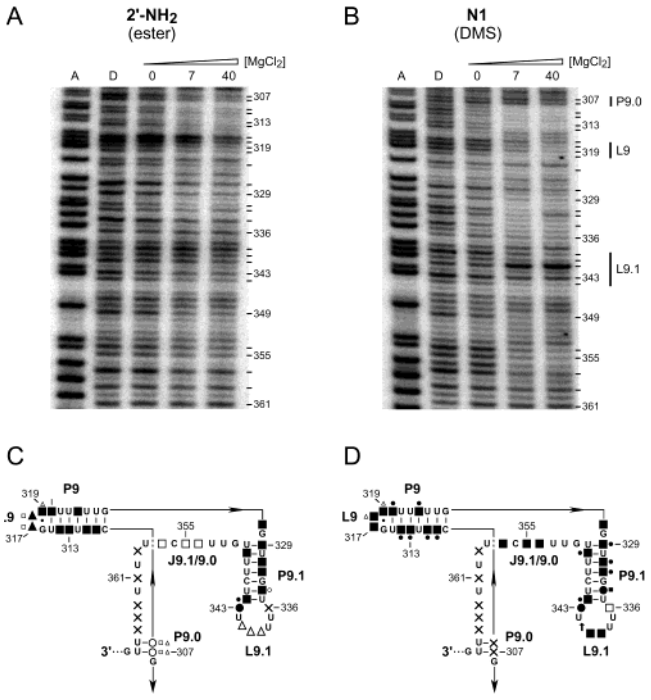

FIGURE 8: Folding of the 3′ region of the bI5 intron. For legend, see Figure 6.

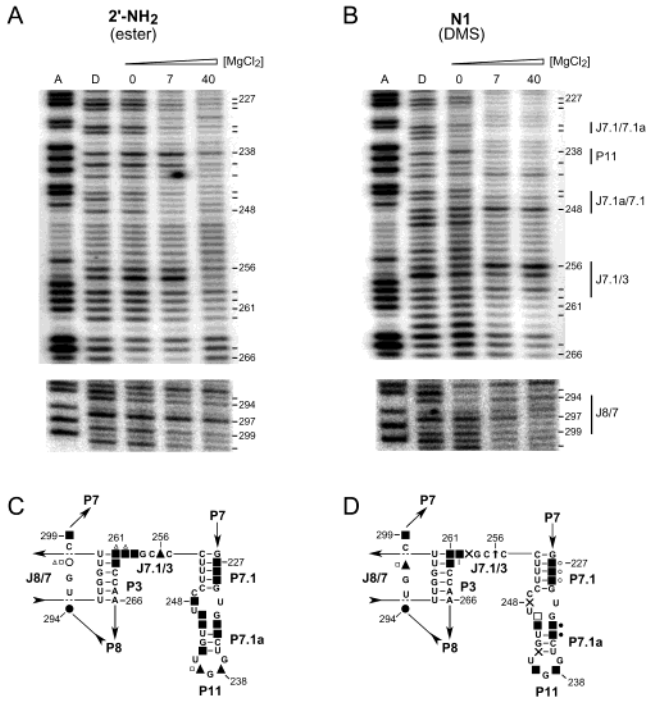

FIGURE 9: Folding of the P3−P7.1 and J8/7 regions of the bI5 intron. For legend, see Figure 6.

second step of splicing (*12*, *26*). The N1 positions of these bases (A306, A307) are accessible to DMS under all conditions tested (Figure 8B). In strong contrast, 2′-amine reactivity progressively decreases in relatively strong transitions at 0 and 7 mM Mg^{2+} (Figure 8A,C). Stable structure formation in this region is also detected as protection from hydroxyl radical cleavage (*15*, *16*) at 40 mM Mg^{2+}. In aggregate, these data support a model for asymmetric assembly (see class 3, Table 2) of the P9.0 helix, in which the two adenosines are pre-organized for binding the UU sequence at the 3′ splice during the second step of splicing.

L9.1 and J9.1/9.0. Both chemistries clearly report that residues in the 5′ portion of the extended J9.1/9.0 region (A354, A355, and A357) show significant protections and are likely to be involved in tertiary interactions. In contrast, residues in the 3′ portion of J9.1/9.0 are reactive and likely unstructured under all conditions tested (see region centered around A361 in Figure 8). A343 is consistently protected from modification by both chemistries at 50 mM KCl, supporting formation of an asymmetric closing A·A pair in P9.1. Other positions in the L9.1 loop show a complex pattern of protection (residues A339−A341, Figure 8). There exists little information to guide analysis of higher order contacts in this region: 2′-amine acylation and N1 methylation protection patterns suggest that this loop forms significant, presently unidentified, tertiary interactions.

J8/7 Bridges the Peripheral and Core Folding Domains. Long-range contacts involving J8/7 are important for stable folding of the catalytic core and for correct docking of the 5′ splice site domain (*12*, *27*, *28*). All adenosine residues in this region are involved in higher order interactions as scored by both 2′-amine acylation and N1 methylation. Interestingly, A294 and A299 show differing stabilities and are protected from either chemistry at 0 versus 7 mM Mg^{2+}, respectively (Figure 9). This suggests that folding at A294 is linked with stable base pairing in P8, whereas A299 folds in the same transition as assembly of the catalytic core (blue squares, Figures 4 and 5). A297, in the center of the J8/7 sequence, exhibits multiple folding transitions, as judged by both mapping chemistries (Figure 9). Because P1 is not docked under these experimental conditions, protection reflects interactions with other elements of the catalytic core.

P3−P7.1−P11 Region. The P7.1−P7.1a helices and the J7.1/3 linking region in the bI5 RNA form an idiosyncratic interaction characteristic of the A1 subgroup of group I introns (*12*, *29*) and are major components of the binding site for the CBP2 protein cofactor (*14*). Two adenosine residues within J7.1/3 are protected from 2′-amine acylation, yet are reactive toward DMS (A256 and A259; Figure 9). These data emphasize that tertiary contacts, independent of the N1 position, form during RNA folding (class 3, Table 2).

Folding transitions for P11 at the base of P7.1a are also different as monitored by 2′-amine acylation and N1 methylation (Figure 9; identified with a dagger in Figures 4 and 5). DMS modification indicates that this helix forms at 7 mM Mg^{2+}; however, the predominant folding transition for 2′-amine acylation occurs at 40 mM Mg^{2+} (Figure 9). A159 on the partner strand in J6a/6b is also protected from DMS at 7 mM Mg^{2+}, but shows progressive protection from 2′-amine acylation in a broad transition from 0 to 40 mM Mg^{2+}. The discrepancy between 2′-amine and N1 modification for P11 is consistent with destabilization of this long-range interaction by 2′-amine substituted nucleotides (class 4A, Table 2).

Protection patterns for 2′-amine acylation and N1 methylation in the regions linking the P7.1 and P7.1a helices are similar and support non-canonical base pairing in this structure (Figure 9, potential base pairing indicated as an extension of the P7.1a helix). One model has stacked A·A and G·A base pairs extending the P7.1a helix (Figure 9C,D)

and A248 forming either a non-canonical pair with U231 or interacting elsewhere in the RNA.

DISCUSSION

Hierarchical Formation of RNA Helices. Analysis of 2′-amine acylation and N1 methylation protection patterns as a function of Mg^{2+} concentration supports the conclusion that base paired helices in the bI5 RNA exhibit two broad classes of stability. Some peripheral helices and a portion of the 5′ domain form stable base pairs at low monovalent ion concentrations (red circles, Figures 4 and 5), whereas essentially all helices in the conserved group I intron catalytic core require Mg^{2+} to form stably (blue squares, Figures 4 and 5). The boundary between helices that form stably at 0 versus 7 mM Mg^{2+} occurs in structurally interesting regions. These include the P1−P2 and P8−P3 junctions and within J8/7.

An overwhelming qualitative conclusion from this work is that 2′-amine acylation scores simple secondary structure formation as reliably as does base methylation by DMS (compare Figures 4 and 5). This is a remarkable conclusion, given that the underlying mechanisms by which these two chemistries detect base pair formation are so different (Scheme 1, Figure 1). The N1 position is resistant to methylation in an A−U base pair because this site is physically occluded from the reagent (Figure 1C). In contrast, a 2′-amine nucleophile is unreactive because nucleotides constrained by base pairing are less able to undergo the "catalytic" conformational change required to juxtapose the 3′-phosphodiester group in the transition state (*11*) (Scheme 1).

Finally, although it is difficult to convey experimental simplicity in figures, we find that 2′-amine acylation is subject to significantly less experimental variability and is easier to implement than DMS modification. This simplicity is due, in part, to parallel hydrolysis of the succinimidyl ester reagent (*9*) that prevents overmodification of the RNA.

Two Classes of Differences between 2′-Amine Acylation and N1 Methylation Chemistries. Almost all differences in reactivity for these two chemistries lie in their sensitivity to non-canonical and higher order interactions. There are two major categories of differences.

The first category consists of residues protected from 2′-amine acylation but not protected from N1 methylation (class 3, Table 2). Representative regions include the sheared A·A base pairs in J4/5, A108 in the A-platform, both adenosines in P9.0, A256 and A259 in J7.1/3, and A248 in J7.1a/7.1.

For the sheared A·A bases in J4/5 and for A108, there is strong structural support (Figure 7A,B, (*22*)) for the conclusion that both chemistries accurately report local structure. A108 is constrained by stacking with G109 and A317 and is therefore relatively unreactive toward 2′-amine acylation; the N1 position is solvent exposed and DMS reactive (Figure 7B).

Similarly, all five adenosine residues in J4/5 are constrained by hydrogen bonding and stacking interactions and are therefore unreactive toward 2′-amine acylation. Four of the A's form two A·A pairs in which one adenosine in each pair is solvent accessible in the wide minor groove and susceptible to DMS modification (Figure 7A). Together, these data suggest that structures in the J4/5 minor groove are pre-organized for docking of the 5′ splice site.

Like J4/5, all of the other class 3 (Table 2) residues lie in regions protected from hydroxyl radical cleavage in the native state (*14*). Our data thus support models for the remaining class 3 residues, in P9.0 and near P7.1, in which these nucleotides participate in tertiary interactions, but the N1 face is accessible. For P9.0, the base pairing faces of these adenosine residues are likely poised for interaction at the 3′ splice site during the second step of splicing.

The second category of dissimilar reactivities involves positions protected from N1 methylation at 0 or 7 mM Mg^{2+}, but where protection from 2′-amine acylation is shifted to higher Mg^{2+} concentrations (compare blue squares and green triangles in Figures 4 and 5). Examples are limited to loops involved in long-range tertiary interactions and include residues in L9, L9.1, and P11. These positions are likely to represent class 4A (Table 2).

Isolated 2′-amino nucleotides favor a C2′-endo conformation (80% C2′-endo), whereas ribonucleotides show a C3′-endo preference (60% C3′-endo) (*30*). This modest C2′-endo preference may destabilize (*10*, *31*) RNA structure in these regions. A more subtle possibility is that the 2′-OH functions as an obligate hydrogen bond donor, which may be compromised by the lower hydrogen bond donating ability of the more basic amine (see ref *32*). In every case in which 2′-amine acylation and N1 methylation chemistries show differing reactivity at 0 or 7 mM Mg^{2+}, protection of the 2′-amine from acylation is eventually observed at 40 mM Mg^{2+}. Thus, most or all tertiary interactions in the bI5 RNA are detectable by 2′-amine acylation under stabilizing folding conditions.

Differential Stability of Helices in the bI5 RNA. There is broad consensus that RNA folding is strongly hierarchical (*33*−*35*), such that the base paired secondary structure forms prior to and is a prerequisite for formation of tertiary interactions. As judged by both 2′-amine acylation and N1 methylation, this work emphasizes an additional hierarchy for formation of base paired secondary structure and other local interactions. Protection patterns for 2′-amine acylation and N1 methylation are superimposed on a three-dimensional model of the bI5 RNA (*14*) in Figure 10 and reveal that peripheral helices that do not interact with other parts of the RNA are more stable than core helices destined to become tightly packed in the native state.

Peripheral structures such as P2−P2a, P6b, P8, and the distal part of P5 are protected from modification in 50 mM monovalent ion (Figure 10, red features). In contrast, most structures containing sequence motifs conserved among group I introns, including the heart of the P5−P4−P6 domain and the P7−P3 helices, require 7 mM Mg^{2+} to be protected from 2′-amine acylation and N1 methylation (Figure 10, blue features).[1] Free energy calculations (*36*) exactly mirror the relative stabilities of stem−loop structures such that the P2a,

[1] We note that the stable helices P6b and P8 are adjacent to artificial deletions in L6b and L8 that yield an RNA with improved folding properties (*18*). However, these engineered loops are placed where loops occur widely among group I introns (*12*) and, for example, P8 in the bI5 RNA is stable in the absence of Mg^{2+} even though residues in the L8 loop are reactive (Figures 4 and 5). In addition, the sequence in P2−P2a is that of the native intron and this peripheral region also forms stable base pairs in the 50 mM KCl folding transition.

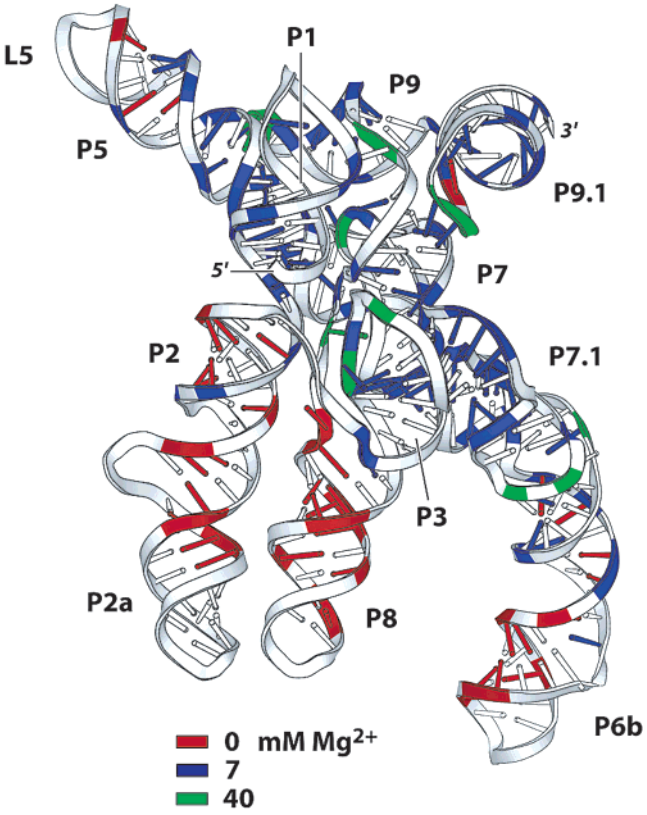

FIGURE 10: External-to-core relative stability of the bI5 group I intron. Colored backbone and cylinders indicate protection from 2′-amine acylation and N1 methylation, respectively, at adenosine residues. Red, blue, and green indicate complete protection at 0, 7, and 40 mM Mg^{2+}, respectively. For residues with multiple folding transitions, the transition at the highest Mg^{2+} concentration is shown. The bI5 RNA model is from ref *14*.

P6b, and P8 helices are more stable ($\Delta G_{37} = -6$ to -9 kcal/mol) than the more reactive P5, P7.1a, P9, and P9.1 helices ($\Delta G_{37} = -2$ to -5 kcal/mol). The greater stability of external helices, not involved in tertiary interactions, may represent a physical constraint for sequences compatible with biological folding of this large RNA.

Consistent with the view that tertiary interactions have the lowest thermodynamic stability and form late in RNA folding, we find (green features in Figures 4, 5, and 10) that residues in L9, L9.1, P11, and J8/7 require the most stabilizing conditions (40 mM Mg^{2+}) to become refractory to modification. Tertiary interactions involving both L9 and A297 in J8/7 form incrementally (Figures 4 and 5), starting under conditions (7 mM Mg^{2+}) where the RNA is in the collapsed state (Table 1). The collapsed state may therefore be partially constrained by native-like tertiary interactions. The equilibrium state for the bI5 RNA, prior to assembly with its protein cofactor, features a relatively loosely packed core anchored by stable external stem−loop structures.

ACKNOWLEDGMENT

We thank G. Bassi, I. Garcia, and K. Buchmueller for helpful discussions and Joe Krahn for assistance with Figure 10.

REFERENCES

1. Wimberly, B., Varani, G., and Tinoco, I., Jr. (1993) *Biochemistry 32*, 1078−1087.
2. Gautheret, D., Konings, D., and Gutell, R. R. (1994) *J. Mol. Biol. 242*, 1−8.
3. Correll, C. C., Freeborn, B., Moore, P. B., and Steitz, T. A. (1997) *Cell 91*, 705−712.
4. Cate, J. H., et al. (1996) *Science 273*, 1696−1699.
5. Doherty, E. A., Batey, R. T., Masquida, B., and Doudna, J. A. (2001) *Nat. Struct. Biol. 8*, 339−343.
6. Nissen, P., Ippolito, J. A., Ban, N., Moore, P. B., and Steitz, T. A. (2001) *Proc. Natl. Acad. Sci U.S.A. 98*, 4899−4903.
7. Peattie, D. A., and Herr, W. (1981) *Proc. Natl. Acad. Sci. U.S.A. 78*, 2273−2277.
8. Ehresmann, C., Baudin, F., Mougel, M., Romby, P., Ebel, J.-P., and Ehresmann, B. (1987) *Nucleic Acids Res. 15*, 9109−9128.
9. Chamberlin, S. I., and Weeks, K. M. (2000) *J. Am. Chem. Soc. 122*, 216−224.
10. John, D. M., and Weeks, K. M. (2002) *Biochemistry 41*, 6866−6874.
11. Chamberlin, S. I., Merino, E. J., and Weeks, K. M. (2002) *Proc. Natl. Acad. Sci. U.S.A. 99*, 14688−14693.
12. Michel, F., and Westhof, E. (1990) *J. Mol. Biol. 216*, 585−610.
13. Golden, B. L., Gooding, A. R., Podell, E. R., and Cech, T. R. (1998) *Science 282*, 259−262.
14. Webb, A. E., Rose, M. A., Westhof, E., and Weeks, K. M. (2001) *J. Mol. Biol. 309*, 1087−1100.
15. Weeks, K. M., and Cech, T. R. (1995) *Cell 82*, 221−230.
16. Buchmueller, K. L., Webb, A. E., Richardson, D. A., and Weeks, K. M. (2000) *Nat. Struct. Biol. 7*, 363−365.
17. Webb, A. E., and Weeks, K. M. (2001) *Nat. Struct. Biol. 8*, 135−140.
18. Weeks, K. M., and Cech, T. R. (1995) *Biochemistry 34*, 7728−7738.
19. Lawley, P. D., and Brookes, P. (1963) *Biochem. J. 89*, 127−138.
20. Gampel, A., and Cech, T. R. (1991) *Genes Dev. 5*, 1870−1880.
21. Costa, M., and Michel, F. (1995) *EMBO J. 14*, 1276−1285.
22. Cate, J. H., et al. (1996) *Science 273*, 1678−1685.
23. Cech, T. R., Damberger, S. H., and Gutell, R. R. (1994) *Struct. Biol. 1*, 273−280.
24. Jaeger, L., Westhof, E., and Michel, F. (1993) *J. Mol. Biol. 234*, 331−346.
25. Strobel, S. A., Ortoleva-Donnelly, L., Ryder, S. P., Cate, J. H., and Moncoeur, E. (1998) *Nat. Struct. Biol. 5*, 60−65.
26. Michel, F., Hanna, M., Green, R., Bartel, D. P., and Szostak, J. W. (1989) *Nature 342*, 391−395.
27. Szewczak, A. A., Ortoleva-Donnelly, L., Ryder, S. P., Monocoeur, E., and Strobel, S. A. (1998) *Nat. Struct. Biol. 5*, 1037−1042.
28. Szewczak, A. A., Ortoleva-Donnelly, L., Zivarts, M. V., Oyelere, A. K., Kazantsev, A. V., and Strobel, S. A. (1999) *Proc. Natl. Acad. Sci. U.S.A. 96*, 11183−11188.
29. Jaeger, L., Westhof, E., and Michel, F. (1991) *J. Mol. Biol. 221*, 1153−1164.
30. Saenger, W. (1984) *Principles of Nucleic Acid Structure*, pp 61−65, Springer-Verlag, New York.
31. Aurup, H., Tuschl, T., Benseler, F., Ludwig, J., and Eckstein, F. (1994) *Nucleic Acids Res. 22*, 20−24.
32. Rablen, P. R., Lockman, J. W., and Jorgensen, W. L. (1998) *J. Phys. Chem. 102*, 3782−3797.
33. Banerjee, A. R., Jaeger, J. A., and Turner, D. H. (1993) *Biochemistry 32*, 153−163.
34. Brion, P., and Westhof, E. (1997) *Annu. Rev. Biophys. Biomol. Struct. 26*, 113−137.
35. Weeks, K. M. (1997) *Curr. Opin. Struct. Biol. 7*, 336−342.
36. Zucker, M., Mathews, D. H., and Turner, D. H. (1999) In *RNA Biochemistry and Biotechnology* (Barciszewski, J., and Clark, B. F. C., Eds.) pp 11−43, NATO ASI Series, Kluwer Academic Publishers.

BI026817H